PNAS
www.pnas.org

Supplementary Information for

Redundancy in synaptic connections enables neurons to learn optimally

Naoki Hiratani, Tomoki Fukai

Naoki Hiratani.

E-mail: N.Hiratani@gmail.com

This PDF file includes:

Supplementary text

Figs. S1 to S2

References for SI reference citations

Supporting Information Text

A conceptual model of multisynaptic learning

The learning rule for multisynaptic connections. In the model, CS (eg. tone stimulus) and US (eg. electric shock) were represented by binary variables $x_n \in \{0,1\}$ and $y_n \in \{0,1\}$. At each trial n, CS was delivered with $\Pr[x_n = 1] = \pi_x$, and US was given only when $x_n = 1$, with probability $\Pr[y_n = 1|x_n = 1] = v_c$. For this task, the update rule for the spine size factor $g_k^{n+1} = \frac{1}{Kq_v(v_k)} p(v_c = v_k|x_{1:n+1}, y_{1:n+1})$ is given as,

$$\begin{aligned} g_k^{n+1} &= \frac{1}{Kq_v(v_k)} p(v_c = v_k|x_{1:n+1}, y_{1:n+1}) \\ &\propto \frac{1}{Kq_v(v_k)} p(x_{n+1}, y_{n+1}|v_c = v_k) p(v_c = v_k|x_{1:n}, y_{1:n}) \\ &\propto p(y_{n+1}|x_{n+1}, v_c = v_k) \left(\frac{1}{Kq_v(v_k)} p(v_c = v_k|x_{1:n}, y_{1:n}) \right) \\ &= p(y_{n+1}|x_{n+1}, v_c = v_k) g_k^n. \end{aligned}$$

In particular, in our problem setting, v_c does not provide any information about y_n when $x_n = 0$, thus assuming $\Pr[y_n = 1|x_n = 0] = 1/2$ (see the proof of convergence below),

$$\begin{aligned} p(y_{n+1}|x_{n+1}, v_c = v_k) &\approx x_{n+1} \left[v_k y_{n+1} + (1 - v_k)(1 - y_{n+1}) \right] + \frac{1}{2}(1 - x_{n+1}) \\ &\propto 1 + (2v_k - 1)x_{n+1}(2y_{n+1} - 1). \end{aligned} \quad [3]$$

Note that due to normalization, the choice of $\Pr[y_n = 1|x_n = 0]$ does not essentially affect the update rule. Because the normalization factor is determined by

$$1 = \int p(v_c'|x_{1:n}, y_{1:n}) dv_c' \approx \frac{1}{K} \sum_k \frac{p(v_c' = v_k|x_{1:n}, y_{1:n})}{q_v(v_k)} = \sum_k g_k^n,$$

the sum of $\{g_k^{n+1}\}$ should also be normalized to 1. Thus the update rule is given as

$$g_k^{n+1} = \frac{[1 + f(x_{n+1}, y_{n+1}; v_k)] g_k^n}{\sum_{k'} [1 + f(x_{n+1}, y_{n+1}; v_{k'})] g_{k'}^n} = \frac{1 + f(x_{n+1}, y_{n+1}; v_k)}{1 + f(x_{n+1}, y_{n+1}; w^n)} g_k^n, \quad [4]$$

where $f(x, y; v) \equiv (2v - 1)x(2y - 1)$ and $w^n \equiv \sum_k w_k^n = \sum_k g_k^n v_k$. As for the resampling process, at every trial n, if spine k satisfied $g_k < g_{th}$, unit EPSP was resampled uniformly from [0,1), and the spine size was set to $g_k = g_{th}$.

Proof of convergence. The derived learning rule can be rewritten as

$$\log p(v_c = v_k|x_{1:n}, y_{1:n}) = \sum_{n'} \log \left[1 + (2v_k - 1)x_{n'}(2y_{n'} - 1) \right] + \text{const},$$

so in order to prove convergence, we need to show that $\varphi(v) \equiv \langle \log \left[1 + (2v - 1)x_{n'}(2y_{n'} - 1) \right] \rangle_{n'}$ is maximized at true v_c. By considering Taylor expansion, the above equation is expanded as $\langle \log(1 + z) \rangle = \sum_{m=1}^{\infty} \frac{(-1)^{m+1}}{m} \langle z^m \rangle$. In this form, the average is calculated as

$$\begin{aligned} \langle ((2v - 1)x_{n'}(2y_{n'} - 1))^m \rangle &= (2v - 1)^m \langle x_{n'} y_{n'} + (-1)^m x_{n'}(1 - y_{n'}) \rangle \\ &= (2v - 1)^m v_c \pi_x + (1 - 2v)^m (1 - v_c) \pi_x \end{aligned}$$

Note that $(x_n)^m = x_n$ if $m > 0$, because $x_n = 0$ or 1. Thus, by substituting the above equation into the Taylor expansion form,

$$\begin{aligned}\varphi(v) &= \pi_x v_c \log\left[1 + (2v-1)\right] + \pi_x(1-v_c)\log\left[1 + (1-2v)\right] \\ &= \pi_x\left[v_c \log v + (1-v_c)\log(1-v)\right] + \text{const.}\end{aligned}$$

Therefore, $\varphi(v)$ is maximized at $v = v_c$.

Monosynaptic learning rule. For comparison, we implemented a monosynaptic learning rule. By expanding the exact solution $\bar{v}_c^n = \sum_{n'} x_{n'} y_{n'} \,/\, \sum_{n'} x_{n'}$:

$$\bar{v}_c^n = \frac{x_n y_n + \sum_{n'=1}^{n-1} x_{n'} y_{n'}}{x_n + \sum_{n'=1}^{n-1} x_{n'}} \approx \bar{v}_c^{n-1}\left(1 + \frac{x_n(y_n - \bar{v}_c^{n-1})}{\sum_{n'=1}^{n-1} x_{n'} y_{n'}}\right).$$

Hence, by using a single variable v_m^n, the learning rule is given as $v_m^n = v_m^{n-1}\left(1 + \eta x_n(y_n - v_m^{n-1})\right)$, where η represents the learning rate. In the optimal learning depicted in Figure 1E, v_c was estimated as $\bar{v}_c^n = (1 + \sum_{n'} x_{n'} y_{n'}) \,/\, (2 + \sum_{n'} x_{n'})$.

Uniform and multinomial rewiring . In the model, we assumed that the unit EPSP of a new synapse is drawn uniformly for biological plausibility. However, such a resampling method is suboptimal as a machine learning algorithm (28,62), and recent experimental results suggest that synaptogenesis is more frequent in active dendritic branches (32). Hence, here we consider an alternative rewiring method based on the multinomial sampling (31).

In this multinomial rewiring method, the unit EPSP v_k of a new synapse is given as $v_k = v_q + \zeta_U$, where index q is probabilistically chosen as $\Pr[q = k'] \propto g_{k'}$, and ζ_U is a uniform random variable taken from [-0.05, 0.05), added to prevent degeneration of synapses (31,62). With this modification, indeed the error keeps decreasing even after 10^5 samples are presented, whereas the performance saturates under a uniform rewiring (Fig. S1A). However, this is partially because due to the absence of weight normalization after each rewiring. If we introduce an explicit weight normalization after each rewiring by $g_k \leftarrow g_k \,/\, \sum_{k'} g_{k'}$, the noise due to rewiring is suppressed, and the difference between two rewiring methods becomes much smaller (Fig. S1B).

Details of the conceptual model. In the simulations, we used $\pi_x = 0.3$, and v_c was randomly chosen from [0,1) uniformly at each simulation (not at each trial). The number of connections was kept at $K = 10$ except for Figure 2B in which $K = 2$ to 20 were used. Initial value of k-th connection v_k was set as $v_k = (k + 0.5)/K$ except for Figure 2C in which the initial distribution was biased by choosing v_k as $v_k = -\log\left(1 - \left[1 - e^{-\lambda_B}\right]\frac{k}{K}\right)$where λ_B is the bias parameter. Resampling was performed with the threshold $g_{th} = 0.0001$, and a new unit EPSP v_k was uniformly sampled from [0,1). In Figure 2B and C, the errors were calculated after learning from 10^4 trials.

Detailed single neuron model

Morphology. We constructed a detailed neuron model based on a model of L2/3 pyramidal neuron with active dendrites (34) using NEURON simulator (33). Here, we used the original reconstructed morphology without scaling. We distributed 1000 excitatory synaptic inputs from 200 presynaptic neurons randomly on the dendrite. Synaptic input was modeled as a double exponential conductance change with the rise time $\tau_{\rm rise} = 0.5$ ms, the decay time $\tau_{\rm decay} = 2.5$ ms, and the reversal potential was set to 0mV. For each synapse k from presynaptic neuron j, we first applied a synaptic input with a constant weight factor $\gamma_g = 2.5$ nS, and then determined the unit EPSP v_j^k of synapse k by measuring somatic membrane potential change. The minimum and the maximum value of the unit EPSP of the given model were $v_{\rm min} = 0.57$ mV and $v_{\rm max} = 2.39$ mV, respectively. In the simulation of the task, using malleable spine size factor g_j^k, we set the weight factor of synapse k as $\gamma_g g_j^k$. Similarly, 200 inhibitory synaptic inputs were uniformly distributed on the dendrite, and the rise and decay time of conductance was set as 0.5ms and 2.5ms, and the reversal potential was set to -90mV. The inhibitory weight factor was chosen as $\gamma_I = 0.75$ nS.

Stimulus selectivity. We hypothesized that all excitatory presynaptic neurons are simple cells having direction selectivity $\{\theta_j\}$ at receptive field (RF) $\{(r_j, \varphi_j)\}$. Here, the position of RF in the visual field was defined by the relative position to the postsynaptic neuron in the polar coordinate (Fig. 3C). We modeled the mean firing rate of presynaptic neuron j for a stimulus θ at the RF of the postsynaptic neuron (i.e. at $r = 0$) as

$$\rho_j(\theta) = \int_0^{2\pi} \rho(\theta'; \theta_j) p(\theta' \text{ at } \{r_j, \varphi_j\} | \theta \text{ at } r = 0) d\theta'.$$

The first term $\rho(\theta'; \theta_j)$ is the mean response of the neuron with orientation selectivity θ_j when orientation θ' is presented at its own RF, hence using a von Mises distribution (63), the response is approximately given as

$$\rho(\theta'; \theta_j) \equiv \frac{\rho_o}{2\pi I_o(\kappa_o)} \exp\left(\kappa_o \cos\left[2(\theta' - \theta_j)\right]\right).$$

The second term is the probability of observing a stimulus with orientation θ' at the position (r_j, φ_j) given stimulus θ at the center. The orientation θ' at (r_j, φ_j) should be similar to the orientation θ at the center if $r_j \sim 0$, or $\varphi_j \sim \theta$ due to continuity and contour statistics (37,38). Hence, we modeled the conditional probability as

$$p(\theta' \text{ at } \{r_j, \varphi_j\} | \theta \text{ at } r = 0) \equiv \frac{1}{2\pi I_o(\kappa_j^r)} \exp\left(-r_j/r_o + \kappa_j^r \cos\left[2(\theta' - \theta)\right]\right)$$

where $\kappa_j^r(\theta) \equiv \frac{r_o}{r_j + r_{\rm min}} \exp(\kappa_\varphi \cos[2(\varphi_j - \theta)])$. Note that the marginalized probability $\exp(-r_i/r_o)$ is smaller than one as an explicit stimulus may not exist at (r_j, φ_j) if the RF is far away from the center. By calculating the integral, the mean firing rate is derived as

$$\rho_j(\theta) = \frac{\rho_o I_o(\tilde{\kappa}_j)}{2\pi I_o(\kappa_o) I_o(\kappa_j^r)} \exp(-r_j/r_o)$$

where $\tilde{\kappa}_j \equiv \sqrt{(\kappa_o)^2 + (\kappa_j^r)^2 + 2\kappa_o \kappa_j^r \cos\left(2[\theta_j - \theta_o]\right)}$. In the simulation, we used $\kappa_o = 2.0$, $\kappa_\varphi = 4.0$, $\rho_o = 1.5\pi$, $r_{\rm min} = 0.01 \exp(\kappa_\varphi)$, and $r_o = 1.0$. The selectivity of each presynaptic neuron was uniformly sampled from the ranges: $0 \le r_j < 3$, $0 \le \varphi_j < 2\pi$, and $0 \le \theta_j < \pi$.

Based on the selectivity described above, we modeled the spiking activity of presynaptic neuron j as a Poisson process with the rate $\rho = \rho_j(\theta)$ under the presence of stimulus $\theta = \theta_+$ or θ_- where $\theta_+ = 0$ and $\theta_- = \pi/2$. In addition,

we assumed that all presynaptic neurons follow a Poisson process with the rate $\rho = \rho_{sp}$ in the spontaneous activity. In the simulation, we set $\rho_{sp} = 0.01\rho_o$.

Task configuration. We next consider the activity of the postsynaptic neuron. A sensory neuron should decode the presented stimulus given stochastic spiking spikes of presynaptic neurons. In particular, here we consider decoding of stimulus orientation θ given spike counts from M presynaptic neurons $s^t_{1:M} = \{s^t_1, s^t_2, ..., s^t_M\}$. As the spikes were generated from Poisson processes in the model, the log-likelihood ratio of $\theta = \theta_+$ against the spontaneous activity ϕ is given as

$$\log \frac{p(\theta_+|s^t_{1:M})}{p(\phi|s^t_{1:M})} = \sum_{j=1}^{M} s^t_j \log\left(\frac{\rho_j(\theta_+)}{\rho_{sp}}\right) + \sum_{j=1}^{M}(\rho_{sp} - \rho_j(\theta_+)) = \sum_{j=1}^{M} w^*_j s^t_j + C., \quad [5]$$

where $w^*_j \equiv \log(\rho_j(\theta_+)/\rho_{sp})$. Hence, if the synapses projected from presynaptic neuron j learn to represent w^*_j jointly, the somatic membrane potential naturally represents the log-likelihood of the stimulus being θ_+, assuming passive dendritic integration.

In this task configuration, the estimated log-likelihoods are on average the same for two perpendicular stimuli $\theta = \theta_+$ and θ_- before learning, but the estimated log-likelihood becomes significantly larger for $\theta = \theta_+$ once the correct weight structure is acquired. Hence, we evaluated the learning performance by a classification between $\theta = \theta_+$ and θ_-, using θ_- as a control.

In the simulation, we first generated the spike counts of each presynaptic neurons $\{s^t_1, s^t_2, ..., s^t_M\}$ by sampling from Poisson distributions with the rates $\{\rho_1, \rho_2, ..., \rho_M\}$ where $\rho_j = \rho_j(\theta_+)$ or $\rho_j(\theta_-)$ depending on the task. Based on the spike count s^t_j, spike timings of the m-th spike from presynaptic neuron j at trial t was determined as $t^{j,t}_m = \left(m - 1 + \zeta^{j,t}_U\right)\Delta t_{\text{stimulus}}/s^t_j$ where $\Delta t_{\text{stimulus}} = 20$ ms, and $\zeta^{j,t}_U$ is a random variable uniformly depicted from [0,1). In the presence of synaptic failure, we instead defined a spike count at each synapse k by $s^t_{j,k} \sim \text{Binomial}(s^t_j, 1 - r_{sf})$, where r_{sf} is the failure rate. Inhibitory spikes were calculated in the same way, but the spike probability was defined by the total excitatory inputs as $\rho^t_{\text{inh}} = \sum_{j=1}^{M} s^t_j/M_{inh}$ to achieve the E/I balance.

The learning rule for the detailed model. We next derived the multisynaptic learning rule for this task. The optimal estimation of the weight from presynaptic neuron j at trial t is given as

$$w^t_j = \int_{w_{\min}}^{w_{\max}} w' \cdot p(w^t_j = w'|s^{1:t}_j, \theta_{1:t})dw' = \int_{v_{\min}}^{v_{\max}} \gamma_w v' \cdot p(w^t_j = \gamma_w v'|s^{1:t}_j, \theta_{1:t})dv'. \quad [6]$$

Here, we introduced a scaling factor γ_w to represent a dimensionless value w by a unit EPSP v [mV]. In the simulation, we used $\gamma_w = w_{\max}/v_{\max}$. By importance sampling,

$$w^t_j = \int_{v_{\min}}^{v_{\max}} \gamma_w v' \frac{p(w^t_j = \gamma_w v'|s^{1:t}_j, \theta_{1:t})}{q(v')} q(v')dv' \approx \frac{1}{K}\sum_{k=1}^{K} \frac{\gamma_w v_{jk} p(w^t_j = \gamma_w v_{jk}|s^{1:t}_j, \theta_{1:t})}{q(v_{jk})} = \gamma_w \sum_{k=1}^{K} g^t_{jk} v_{jk},$$

where $g^t_{jk} \equiv p(w^t_j = \gamma_w v_{jk}|s^{1:t}_j, \theta_{1:t}) \,/\, (Kq(v_{jk}))$ represents the relative spine size of spine k from presynaptic neuron j, and K is the total number of synapses per presynaptic neuron. Therefore, considering a Bayesian filtering, the update of $\{w^t_j\}$ is done by the following update of spine size $\{g^t_{jk}\}$

$$\tilde{g}^t_{jk} = g^t_{jk} \cdot p(s^t_j|\theta_t, w_j = \gamma_w v_{jk}), \quad g^{t+1}_{jk} = \tilde{g}^t_{jk} \,/\, \sum_{k'} \tilde{g}^t_{jk'}, \quad [7]$$

where

$$p(s_j^t|\theta_t, w_j = \gamma_w v_{jk}) = \frac{\delta(\theta_t = \theta_+)}{s_j^t!} \exp\left([\gamma_w v_{jk} + \log \rho_{sp}]\, s_j^t - \rho_{sp} e^{\gamma_w v_{jk}}\right) + \frac{\delta(\theta_t \neq \theta_+)}{s_j^t!} \exp\left(s_j^t \log \rho_{sp} - \rho_{sp}\right) \quad [8]$$

and $\delta(x)$ is a function that returns 1 if x is true, but returns 0 otherwise. In particular, if $\theta_t = \theta_+$ and $s_j^t = 1$, then $\tilde{g}_{jk}^t$ is multiplied by the factor of $\rho_{sp} \exp\left(\gamma_w v_{jk} - \rho_{sp} e^{\gamma_w v_{jk}}\right)$, that typically causes potentiation. On the other hand, if $\theta_t = \theta_+$ and $s_j^t = 0$, then $\tilde{g}_{jk}^t$ is depotentiated by the factor of $\exp\left(-\rho_{sp} e^{\gamma_w v_{jk}}\right)$, resembling a Hebbian rule. Note that g_{jk}^t does not change if $\theta \neq \theta_+$, because the change due to the second term of Eq. 8 is canceled out at the normalization due to the lack of v_k dependence.

At every trial, synapses with spine size $g_{jk}^t < g_{th}$ was removed with 20% chance. If a synapse is removed, a new synaptic contact from the corresponding presynaptic neuron was simultaneously created on one of the dendritic branches to which the neuron initially had projections. Probability of selecting a branch was set to be proportional to the length of the branch. Spine size of a newly created synapse was set to $g_{jk}^t = 1/K$. This rewiring procedure is slightly different from the one in the conceptual model, because rewiring becomes too frequent if we directly apply the latter.

In addition to rewiring of synaptic connections, we also included an elimination process that is not compensated by new connections, as the total number of synaptic connections is known to decreases during development (30). In particular, inactive synapses are expected to be more fragile (64). Hence, we tracked the firing rate of presynaptic neuron during the training phase by $r_j^t = (1 - 1/\tau_r) r_j^{t-1} + s_j^t/\tau_r$. At every trial, if the presynaptic firing rate satisfies $r_j^t < r_{\text{el-th}}$, we eliminated the synaptic contact with 20% chance. Throughout the simulation, we used $g_{th} = 0.001$, $\tau_r = 10.0$, and $r_{\text{el-th}} = 0.05$.

Monosynaptic learning rule for the detailed model. As presynaptic neurons follow stationary Poisson processes, the learning rule for monosynaptic connection was defined as

$$g_j^t = g_j^{t-1} + \eta_w \left(s_j^t \exp[-2\gamma_w v_j] - \rho_{sp}\right), \quad [9]$$

where η_w is the learning rate parameter (17,51), and v_j is the unit EPSP of the synaptic connection from neuron j. To ensure stability, we bounded the spine size between $0 < g_j^t < 1$, and doubled the scaling factor from γ_w to $2\gamma_w$.

Presynaptic stochasticity . It is known that presynaptic release probability tends to match with postsynaptic spine size (44,45), although exact nature of pre- and postsynaptic change in synaptic plasticity is still controversial (54). Hence, the synaptic factor g_k might be cooperatively expressed by presynaptic release probability b_k and the postsynaptic factor a_k, instead of the purely postsynaptic representation assumed in the main result. In particular, under the pre-post matching, b_k and a_k can be defined as

$$b_k = \begin{cases} b_o \sqrt{K g_k} & (\text{if } g_k \leq \frac{1}{K b_o^2}) \\ 1 & (\text{otherwise}) \end{cases}, \quad a_k = \begin{cases} \frac{1}{b_o} \sqrt{\frac{g_k}{K}} & (\text{if } g_k \leq \frac{1}{K b_o^2}) \\ g_k & (\text{otherwise}) \end{cases}. \quad [10]$$

This matching is potentially beneficial for the readout of the uncertainty in the synaptic representation of the decoding model. The variance in the somatic EPSP caused by the presynaptic stochasticity is written as $\left\langle \left(\sum_k a_k (B_k - b_k)\right)^2 \right\rangle =$

$\sum_k a_k g_k - \sum_k g_k^2$, where B_k is a binary random variable. Considering a sublinear dependence of a_k on g_k, the somatic variance may show a negative dependence on the synaptic variability $\sum_k g_k^2$. Importantly, the second moment of the synaptic factors $\sum_k g_k^2$ increases as the neuron learns the task (Fig. 4K), because small number of synapses are potentiated while others are depotentiated during learning (see also Fig. 3H). This means that the somatic EPSP variance due to presynaptic stochasticity tends to decrease during learning, enabling more precise spike generation and more reliable information transmission.

On the other hand, if the release probability is kept constant for all the synapses ($b_k = b_o$) as in Figure 5D, then the somatic variance is given as $\left\langle \left(\sum_k a_k (B_k - b_k)\right)^2 \right\rangle = b_o(1-b_o)\sum_k g_k^2$. Thus, the variability in the somatic membrane potential linearly increases as the variance of $\{g_k\}$ increases, causing additional noise as the neuron learns the task. Another interesting scenario is the purely presynaptic representation ($b_k \propto g_k$). In this case, the somatic EPSP variance is described as $a_o - \sum_k g_k^2$ using a constant value a_o, but it is unclear if this scenario is biologically relevant.

Implementing it into the detailed neuron model, with the pre-post matching, the Fano factor of the maximum somatic EPSP height went down as the performance improved (Fig. S2B). On the contrary, the fano factor increased in the model with a constant release probability, though the performance was somewhat better (Fig. S2A). Here, we used the Fano factor instead of the variance, because the mean somatic EPSP height typically decreased during learning due to a shift in the E/I balance. The Fano factor was estimated by presenting a frozen presynaptic spike pattern while changing the number of transmitted spikes at each synaptic contact stochastically. In addition, we used the following synaptic update rule by explicitly taking account of the presynaptic stochasticity, whereas a naive scaling (i.e. $b_{jk} = 1$) was used in Figure 5D.

$$\begin{aligned} p\left(s_{jk}^t | \theta_+, w_j = \gamma_w v_{jk}\right) &= \sum_{s_j = s_{jk}^t}^{\infty} p\left(s_{jk}^t | s_j\right) p\left(s_j^t | \theta_+, w_j = \gamma_w v_{jk}\right) \\ &= \sum_{s_j = s_{jk}^t}^{\infty} \binom{s_j}{s_{jk}^t} \left(b_{jk}\right)^{s_{jk}^t} \left(1 - b_{jk}\right)^{s_j - s_{jk}^t} \frac{1}{s_j!} \exp\left(\left[\gamma_w v_{jk} + \log \rho_{sp}\right] s_j - \rho_{sp} e^{\gamma_w v_{jk}}\right) \\ &= \frac{1}{s_{jk}^t!} \exp\left(\left[\gamma_w v_{jk} + \log\left(b_{jk}\rho_{sp}\right)\right] s_{jk}^t - b_{jk}\rho_{sp} e^{\gamma_w v_{jk}}\right). \end{aligned}$$

The surrogate learning rule. In the surrogate rule, each synapse estimates the mean unit EPSP by $v_{jk}^o = (1 - g_{jk}^t)v_o + g_{jk}^t v_{jk}$, where v_o is the standard unit EPSP. Subsequently, a synapse updates its spine size by

$$\begin{aligned} g_{jk}^{t+1} &= g_{jk}^t \exp\left(s_j^t \log\left[\rho_{jk} \,/\, \rho_{jk}^{o,t}\right] - \left[\rho_{jk} - \rho_{jk}^{o,t}\right]\right) / \, Z_t, \\ Z_t &= \exp\left[\frac{1}{MK}\sum_{j,k}\left(s_j^t \log\left[\rho_{jk} \,/\, \rho_{jk}^{o,t}\right] - \left[\rho_{jk} - \rho_{jk}^{o,t}\right]\right)\right], \end{aligned} \qquad [11]$$

given a horizontal stimulus, where $\rho_{jk} = \rho_{sp}\exp\left(\gamma_w v_{jk}\right)$, $\rho_{jk}^{o,t} = \rho_{sp}\exp\left(\gamma_w v_{jk}^{o,t}\right)$. The normalization term Z_t is global in a sense that the term is given by the summation over all the excitatory synapses projected to the postsynaptic neuron. To ensure the stability, we bounded the spine size factor as $0 \le g_{jk}^t \le 1/2$, and set $v_o = 1.5 v_{\min} (\approx 0.9\text{mV})$.

Performance evaluation. During the training phase, only the target (i.e. horizontal stimulus $\theta = \theta_+$) was presented. In the test phase, we presented 200 stimuli, of which 100 stimuli were the horizontal stimulus ($\theta = \theta_+$), while the other half were the vertical stimulus ($\theta = \theta_-$). In Figure 3F, 5A, 5B and 5E, we stopped the training at every 10

trials, and measured the performance. The classification performance was measured by the ratio of horizontal trials in which the maximum EPSP height exceeded the threshold $v_\theta = \left(m_h/\sigma_h^2 + m_v/\sigma_v^2\right) / \left(1/\sigma_h^2 + 1/\sigma_v^2\right)$, to the total of 100 trials, where $m_h = \mathrm{E}[\Delta v_n^h]$ and $\sigma_h^2 = \mathrm{Var}[\Delta v_n^h]$ were calculated over 100 test stimuli (n=1, 2, ...,100). Although the evaluations were made solely on false negatives, we also observed significant decrease of false positives during learning (Fig. 3E). When a postsynaptic action potential was emitted, we used the estimated membrane threshold $\Delta v_{th} = 25$ mV as the maximum EPSP height Δv_n, but such a trial was rare (<1%) in our model setting.

Details of the NEURON simulations. Initial values of spine sizes $\{g_j^k\}$ were chosen such that $g_j^k \sim 1/q_v(v_j^k)$ is satisfied. To this end, we first estimated the unit EPSP density at $v = v_j^k$ through a sample-based approximation:

$$q_v(v_j^k) \propto \sum_{m=1}^{M} \sum_{i=1}^{K} \delta\left[v_j^k - dv/2 \le v_m^i < v_j^k + dv/2\right] \equiv \tilde{q}_v(v_j^k)$$

where $dv = (v_{\max} - v_{\min})/10$. Then we calculated g_j^k by $g_j^k = \frac{1/\tilde{q}_v(v_j^k)}{\sum_{k'} 1/\tilde{q}_v(v_j^{k'})}$. In Figure 5A, to generate a biased synaptic distribution, we randomly sampled a position from the whole dendritic tree with probability $\frac{1}{10B(\lambda_B, 2-\lambda_B)} \left(\frac{L'}{L_{\max}}\right)^{\lambda_B - 1} \cdot \left(1 - \frac{L'}{L_{\max}}\right)^{1-\lambda_B}$, and added a synapse until 1000 synapses are created on the dendritic tree. Here, L' is the distance from the soma, $L_{\max}$ is the maximum distance, λ_B is the bias parameter, and $B(x, y)$ is the Beta function. Presynaptic selectivity and initial synaptic contacts were randomly generated for each simulation, while the dendritic morphology was fixed. Further details of the model are available at ModelDB (http://modeldb.yale.edu/225075).

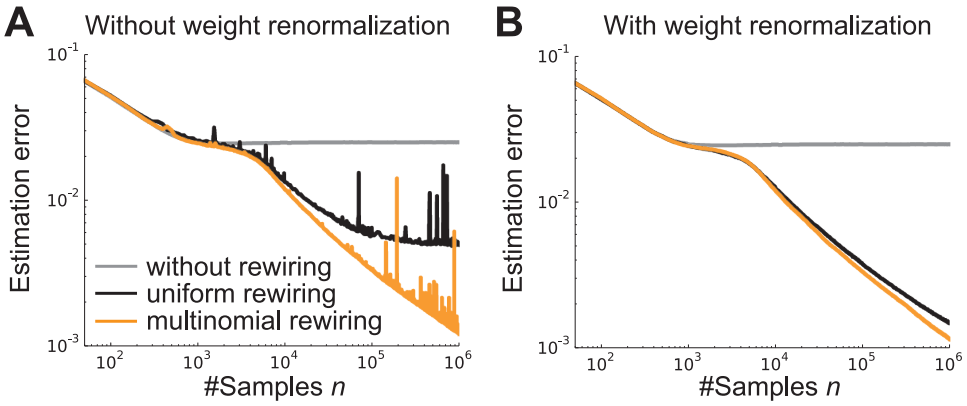

Fig. S1. Comparison of uniform and multinomial rewiring. **A)** Performance curves under large number of samples. Gray and black lines are models without rewiring and with uniform rewiring, respectively as in Figure 2, whereas the multinomial rewiring was used for the orange line (see *uniform and multinomial rewiring* in SI). **B)** Same with **A**, but with weight normalization $\left(g_k \leftarrow g_k \,/\, \sum_{k'} g_{k'}\right)$ after each rewiring.

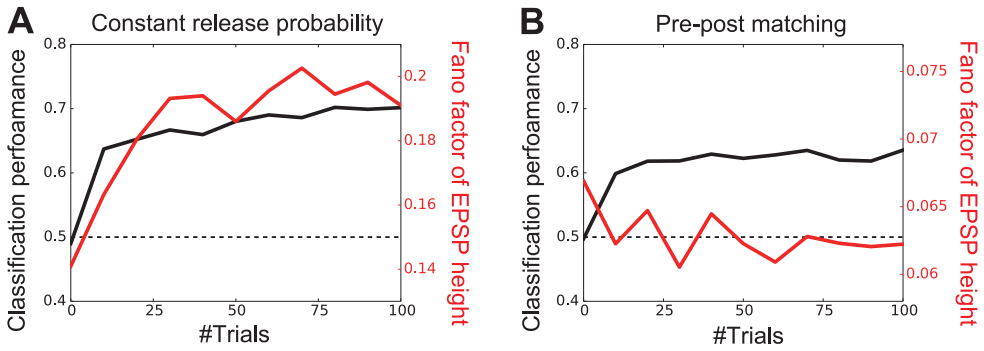

Fig. S2. Constant and matched presynaptic release probability **A)** The development in classification performance (black line), and the Fano factor of the maximum somatic EPSP height (red line) under a constant release probability $(1 - r_{\text{sf}} = 0.66)$. **B)** The same, but under a model with pre-post matching. In the simulation, we set $b_o = 0.75$ to keep the average release probability at $\langle b_{jk} \rangle \approx 0.66$. In both panels, the lines are the means over 50 simulations, and the Fano factor was calculated from the mean and the variance over 20 presentations of the same spike pattern with variability due to stochastic synaptic transmission.

References

62. Gordon NJ, Salmond DJ, Smith AFM (1993) Novel approach to nonlinear/non-Gaussian Bayesian state estimation. IEE Proc F Radar Signal Process 140(2):107-113.
63. Swindale NV (1998) Orientation tuning curves: empirical description and estimation of parameters. Biol Cybern 78(1):45-56.
64. Wiegert JS, Oertner TG (2013) Long-term depression triggers the selective elimination of weakly integrated synapses. Proc Natl Acad Sci U S A 110(47):E4510-4519.